A Study on the Use of Kilohertz Acoustic Energy for Aluminum Shaping and Mass Transport in Ambient Condition Metal 3D Printing

by

Anagh Deshpande

A Thesis Presented in Partial Fulfillment
of the Requirements for the Degree
Master of Science

Approved July 2016 by the
Graduate Supervisory Committee:

Keng Hsu, Chair
Hanqing Jiang
John Parsey

ARIZONA STATE UNIVERSITY

August 2016

ABSTRACT

This research work demonstrates the process feasibility of Ultrasonic Filament Modeling process as a metal additive manufacturing process. Additive manufacturing (or 3d printing) is the method to manufacture 3d objects layer by layer. Current direct or indirect metal additive manufacturing processes either require a high power heat source like a laser or an electron beam, or require some kind of a post processing operation to produce net-shape fully-dense 3D components. The novel process of Ultrasonic Filament Modeling uses ultrasonic energy to achieve voxel deformation and inter-layer and intra-layer mass transport between voxels causing metallurgical bonding between the voxels. This enables the process to build net-shape 3D components at room temperature and ambient conditions. Two parallel mechanisms, ultrasonic softening and enhanced mass transport due to ultrasonic irradiation enable the voxel shaping and bonding respectively. This work investigates ultrasonic softening and the mass transport across voxels. Microstructural changes in aluminium during the voxel shaping have also been investigated. The temperature evolution during the process has been analyzed and presented in this work.

ACKNOWLEDGMENTS

I sincerely thank my advisor, Professor Keng Hsu, for providing me an opportunity to work on the Ultrasonic Filament Modeling project. The project has been a steep learning curve for me. The long sessions of discussions with him have always been insightful. His consistent support and help have made this work possible.

I would also like to thank Professor Hanqing Jiang and Professor John Parsey for taking some time from their busy schedule to be a part of my supervisory committee.

I would like to thank Professor Sangram Redkar for lending me some of his expensive equipment to carry out a few experiments and Mr. Osama Jameel and Mr. Rhett Sweeney for their help and support with my work. I would also like to thank my lab mates for their help and for making the time in the lab a little fun.

Finally, I would like to thank all my friends and family for all their help and support.

TABLE OF CONTENTS

CHAPTER Page

LIST OF FIGURES

Figure Page

Figure Page

1. INTRODUCTION

American Society for Testing and Materials defines additive manufacturing (or 3D printing) as “the process of joining materials to make objects from 3D model data, usually layer upon layer”. The technology was perceived as a mere prototyping tool (hence the alias rapid prototyping) during its inception. But over the last decade, the technology has graduated from being a mere prototyping tool to being a preferred tool of choice in many cases for producing end-use components [1]. It Is revolutionizing the way things are manufactured and is penetrating into every type of manufacturing industry like aerospace, automobiles, bio-medical, military, electronics, consumer goods, foods and personal products. The distinct advantages of additive manufacturing are [2]-

1) No tooling is needed significantly reducing production ramp up time and expense
2) Small production batches are feasible and are economical
3) Possibility to quickly change design
4) Allows product to be optimized for function
5) Allows economical custom products
6) Possibility to reduce waste
7) Potential for simpler supply chains; shorter lead times, lower inventories
8) Design customization.

All of these advantages make additive manufacturing a lucrative choice in today’s fast changing markets which compel companies to produce low-volume, personalized, innovative and sustainable products. Over the last decade, extensive research and convenience of process physics has led to the development of low and medium-cost polymer 3D printing technologies like Fused Deposition Modeling (FDM), Stereolithography (SLA), Multi-Jet Modeling (MJM), etc. that are capable of producing production quality components [3]. This has made polymer additive manufacturing affordable. However, additive manufacturing of fully-dense metals is still far from being affordable and accessible [4].

Current metal additive manufacturing technologies include indirect methods such as Binder Jet processes, Ultrasonic Consolidation (UC) and Laminate Object Manufacturing (LOM) and direct methods like Selective Laser Melting (SLM), Electron Beam Melting (EMB) and Laser Engineered Net Shaping (LENS) [3]. All indirect methods require post-processing to produce fully dense parts. Ultrasonic Consolidation is a hybrid additive-subtractive process where sheets (or strips) of metal foils are first ultrasonically welded into a stack. A cutting operation (often end-milling) is then used to shape the metal stack into the desired layer shape. By alternating between these welding and cutting processes, 3-dimensional objects are constructed. LOM follows the same alternating adding and cutting process as UC, but the welding steps are replaced by adhesives applied between sheets, and a post-fabrication sintering process may be required.

All direct metal additive manufacturing processes use a high power thermal source such as a laser or an electron beam to melt and bond metal powder particles together. Disadvantages of the current metal additive manufacturing processes are-

1) The resulting structures, micro-structures and morphology of the components built using these technologies depend highly on the thermal-physical and heat-transfer processes during the micro-welding event and hence are very difficult to manipulate and control [5].
2) These technologies use powder as the starting material, typically 20 micrometer or so in mean diameter. Hence, the process has to take place in a controlled environment of inert gases or vacuum to prevent oxidation, beam scattering in the case of electron beam melting and other process hazards.
3) All of these characteristics make these technologies inaccessible to small and medium scale manufacturers.

Ultrasonic Filament Modeling

Ultrasonic Filament Modeling, developed and studied through this research work, is a novel approach that can additively manufacture fully-dense (<95%) metal components at room temperature and in ambient conditions. The working principle of this process can be thought of as the marriage of Wire Bonding and Fused Deposition Modeling: a solid metal filament is used as

the starting material to form a fully-dense 3 dimensional object via the metallurgical bonding between the roads and layers with the help of ultrasonic energy. The use of ultrasonic energy reduces the mechanical stress (and therefore mechanical energy input) required to “shape” the filament into the desired road geometry drastically (< 50%) below the yield strength of the material. This is referred to as ultrasonic softening. The amount of mass transport across the inter-filament and inter-layer interfaces to form the metallurgical bonds observed is more than 10,000 times higher [6] than what Fick’s diffusion predicts under the observed conditions. Due to these characteristics, UFM has several advantages over the current metal additive manufacturing processes-

1) It can be stand-alone metal 3D printing process which can manufacture fully dense components that does not require post processing.
2) It uses filaments as starting material instead of powder in the processes like SLS or EBM. This eliminates the process hazards associated with the oxidation of metal powder
3) It can operate at ambient conditions and room temperature
4) Being a room temperature and ambient condition process, it can be implemented in a desktop 3D printing environment
5) It can be used in combination with a polymer additive manufacturing process to produce metal-polymer composites that otherwise might not be possible with current metal 3D printing temperatures due to their high operating temperatures.
6) It has the potential to offer a cost effective alternative to current metal 3D printing processes

Outline of the Thesis

- Chapter 1 gives a brief introduction of additive manufacturing, current metal additive manufacturing processes and their drawbacks. It then introduces Ultrasonic Filament Modeling and its advantages over the current metal additive manufacturing processes.
- Chapter 2 presents a literature review of the prior art on wire bonding, ultrasonic softening and enhanced mass transport due to ultrasonic irradiation.

- Chapter 3 talks about the experimental setup of the UFM process. It also outlines the sample preparation and experiments performed to study the ultrasonic induced. microstructural changes after voxel formation and also to study the enhanced mass transport across voxels. The infra-red camera setup to study the temperature evolution during the voxel formation and bonding process has also been explained in this chapter.
- Chapter 4 presents the results of the experiments conducted.
- Chapter 5 analyzes, interprets and discusses the results.
- The future work necessary to advance this process and to further understand its process physics has been outlined in Chapter 6.
- The thesis report is concluded in Chapter 7 with the summary.

2. LITERATURE REVIEW

The physical phenomena that enable Ultrasonic Filament Modeling are attributed to the well observed ultrasonic softening of metals, and a second lesser studied mechanism that involves a drastically enhanced mass transport (4-6 orders of magnitude) at the lattice level.

The acoustic softening effect was first identified in the 1950s and is believed to be due to the lowered activation energy to dislocation gliding as a result of acoustic energy concentrated at lattice defects such as dislocations and grain boundaries. Langenecker [7] demonstrated the reduction in the yield stress during the deformation of aluminum under the simultaneous application of ultrasonic energy. The effect was similar to thermal energy effect, but the amount of ultrasonic energy density required to attain similar reduction in yield stress was 10^7 times less

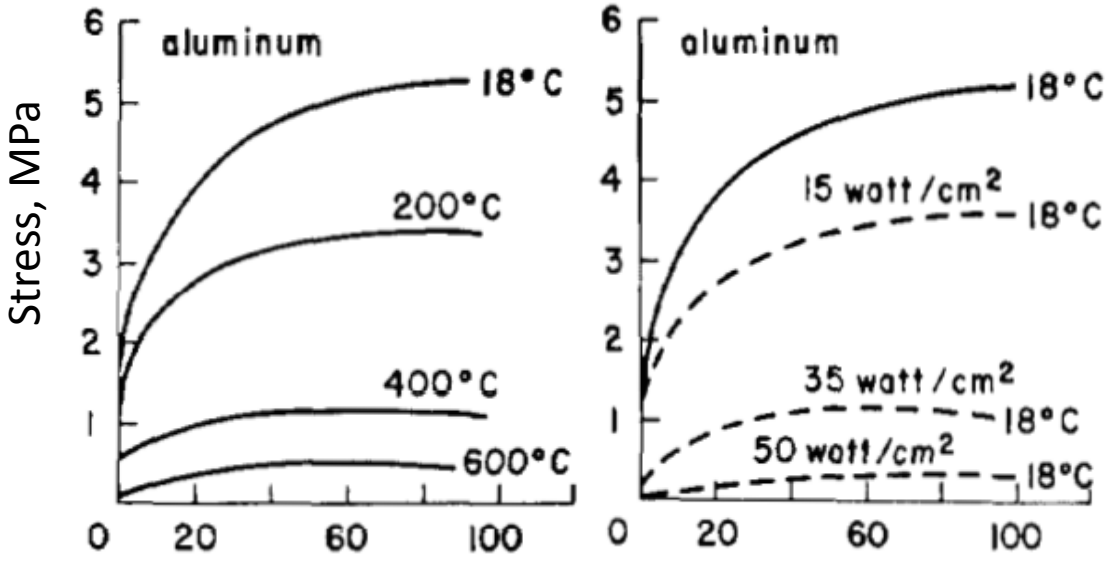

Figure 1: Comparison of the Effect of Heat Energy and Ultrasonic Energy on the Deformation Curve of Aluminum [7]

than thermal energy due to preferential absorption of ultrasonic energy at the dislocations. Figure 1 shows the comparison of the effect of heat and ultrasonic energy on the deformation curve of aluminium.

In more recent studies, significant amount of research has gone into modelling the effect of ultrasonic energy on the deformation characteristics of metals. Rusinko [8] introduced a new term

called ultrasonic defect density to account for the transient ultrasonic softening and residual hardening. Siddiq and Sayed in [9] modified the porous plasticity model to account for the ultrasonic softening effects during ultrasonic assisted manufacturing processes like forming and wire-drawing. Yao et al. [10] modified the crystal plasticity frame work to model the ultrasonic softening and residual hardening during the upsetting experiments.

Similar process physics involving ultrasonic softening and enhanced mass transport is being widely used in wire bonding process in the micro-electronic packaging industry. The purpose of wire bonding process is to establish electrical contact between two metallic surfaces. Harman [11] and Joshi [12] analyzed the heat evolution during the wire bonding process to conclude that the maximum temperature rise during the process is less than 60^0 C. They attributed this to the negligible relative motion between the wire and the substrate which minimizes the frictional heat generation. Due to this, the softening and mass transport is fully governed by ultrasonic energy without any influence of frictional heat energy.

In current literature the observations of the drastically increased mass transport behavior on a material interface in the kHz range has primarily been in the context of the Wire bonding processes. Li et al. [13] bonded gold wires to aluminum substrates and measured the interface thickness using Transmission Electron Microscopy images of the cross-section. Energy Dispersive Spectroscopy (EDS) analysis of interface zone indicated the presence of inter-metallic compound Au_4Al. Figure 2 shows the EDS results along the line on vertical section of Au/Al bond. Along with the changes in composition, increase in the dislocation density was also observed. Others [14] have also performed similar TEM studies of the bond interfaces and made similar observations. Yet detailed explanations of the mechanics of the phenomenon have not been made.

Ultrasonic Consolidation (UC) is a hybrid additive-subtractive process where sheets (or strips) of metal foils are first ultrasonically welded into a stack. A cutting operation (often end-milling) is then used to shape the metal stack into the desired layer shape. Unlike UFM, large temperature rise of the order of several hundred degrees has been observed during UC [15]. This difference in

the two processes can be attributed to the difference in the aspect ratio of cross-section of foils used in UC (10 to few 100) and the filaments used in UFM (aspect ratio of 1). This results in a major difference in process mechanics due to the completely different strain field in the material. In the UFM process, the mass transport and softening is purely due to acoustic energy coupling, whereas the effect of heating is not negligible in UC.

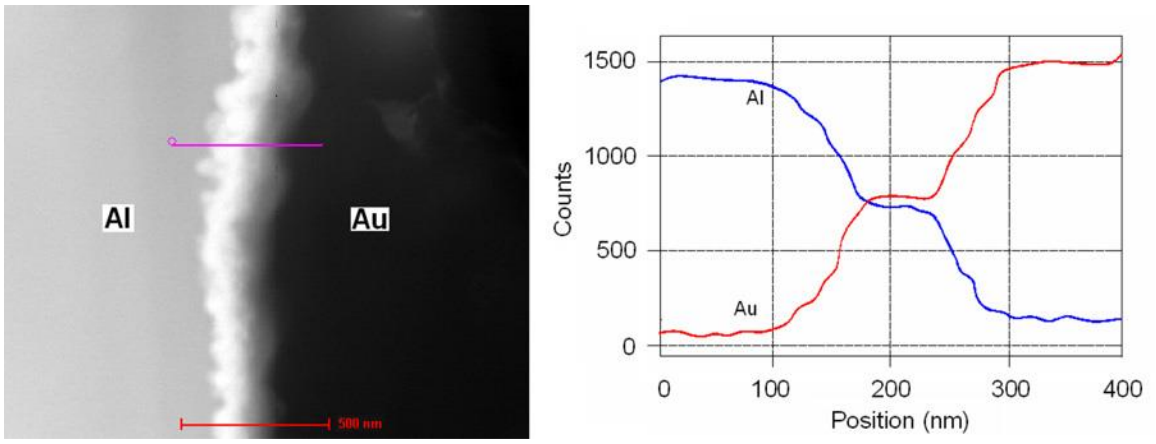

Figure 2: EDS Results of the Cross Section of Au/Al Interface After Wire Bonding [11]

In the Ultrasonic Consolidation domain, Siddiq and Ghassemieh [16] included the softening effect of frictional heat during UC in their model along with the ultrasonic softening effect to analyze the softening during the UC process. Kelly et al. [15] found an empirical relation to calculate the percent softening term from the dimensionless ultrasonic vibration amplitude and pressure during UC. Sietins et al. [17] performed transmission electron microscopy of an ultrasonically consolidated copper-aluminium interface. The large amounts of mass transport across material interfaces was observed but with much higher temperature increases. The exact governing mechanism of enhanced mass transport under the influence of ultrasonic irradation still remains an open question.

UFM has some significant advantages over UC. UFM is a stand-alone process and does not require a post-processing machining operation. Since UFM is a room temperature process, it can be combined with polymers or other low melting temperature materials to create hybrid materials. due to the use of filaments with small contact area, the mechanical loads used in the UFM

process is orders of magnitude smaller than what is required in the UC process. Due to this, UFM can be implemented in a desktop printing environment.

Along with the ultrasonic softening during UFM, characteristics of dynamic recovery were also observed in the microstructure of the deformed filament, even though the process takes place at room temperature. Dynamic recovery is the dynamic restoration process operating during the hot deformation ($T>0.5T_m$) of high stacking fault energy materials like aluminum, ferritic iron, Mg, etc. [18]. In [19], subgrain formation was reported after micro and nano-indentation experiments under ultrasonic irradiation using TEM micrographs. Subgrain formation indicates dynamic recovery as the restoration process in [19]. This can be used to manipulate the microstructure of the component being 3D printed in real-time during the UFM process.

3. EXPERIMENTAL SETUP AND DESIGN

Experimental Setup for UFM Process

Figure 3 shows the schematic diagram of the experimental setup for UFM. A stainless steel horn is connected to a piezoelectric crystal that vibrates at a frequency of 60 kHz. The vibration amplitude of the machine can be adjusted to change the power of the ultrasonic energy. A tungsten carbide tool is attached to the end of the horn. 300 µm filament (99.99% Al) is fed under the tool through a capillary. The tool vibrates in the direction parallel to the axis of filament. The tip of the tool is flat (1mmx1mm). The substrate used is rolled 1100 aluminum. The parameters that affect the strength of bond between the filament and the substrate (or lower layer) and can be controlled on the setup are 1) power of the ultrasonic energy by changing the amplitude of vibration, 2) time for which the ultrasonic energy is applied and 3) force that the tool exerts on the filament.

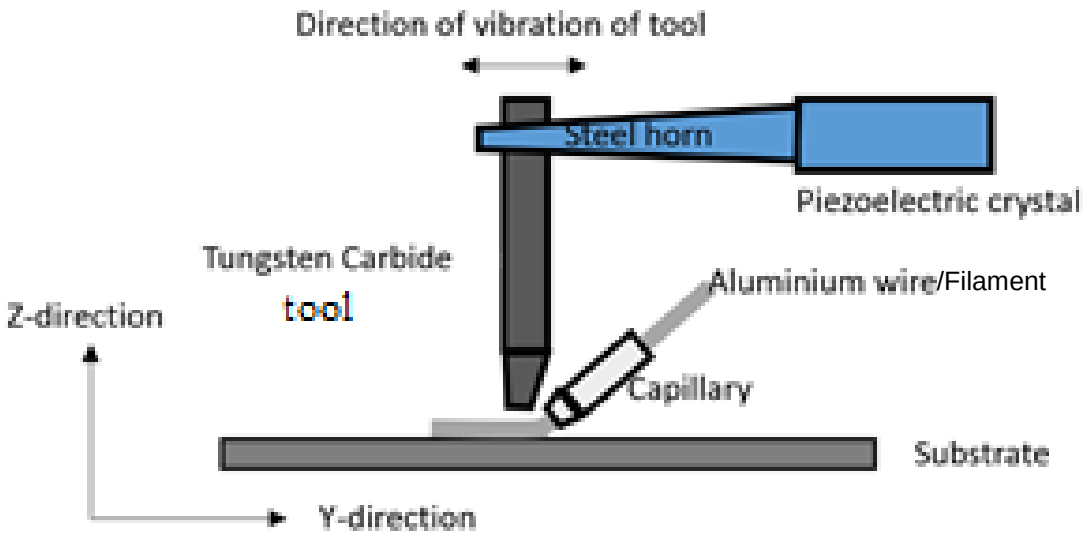

Figure 3: Schematic Diagram of the Experimental Setup for UFM

Methodology for UFM Process

First, the tool is brought down to exert a force on the filament. At the same time, ultrasonic energy is supplied to the tool. Ultrasonic energy results in reduction in the yield stress of the aluminium filament and the filament plastically deforms. The plastic deformation coupled with enhanced mass transport results in the filament getting bonded to the aluminium substrate. Immediately after the bond is completed, the tool moves up. The substrate is moved in the Y-direction and the second bond is made. Some part of the tool overlaps the first bond. This process is continued until the desired length of filament is bonded to the substrate. The overlap between each discrete bonds results in a continuous filament being bonded to the substrate. Similarly, another filament is bonded to the substrate adjacent to the earlier bonded filament. The process is repeated until the desired width is achieved. This results in a layer of aluminium being built on the substrate. On top of this layer, several layers can be built to achieve a 3D geometry. Figure 4 shows the schematic diagram when the 2nd layer is being built and Figure 5 shows the SEM image of the cross-section after two layers have been built on the substrate.

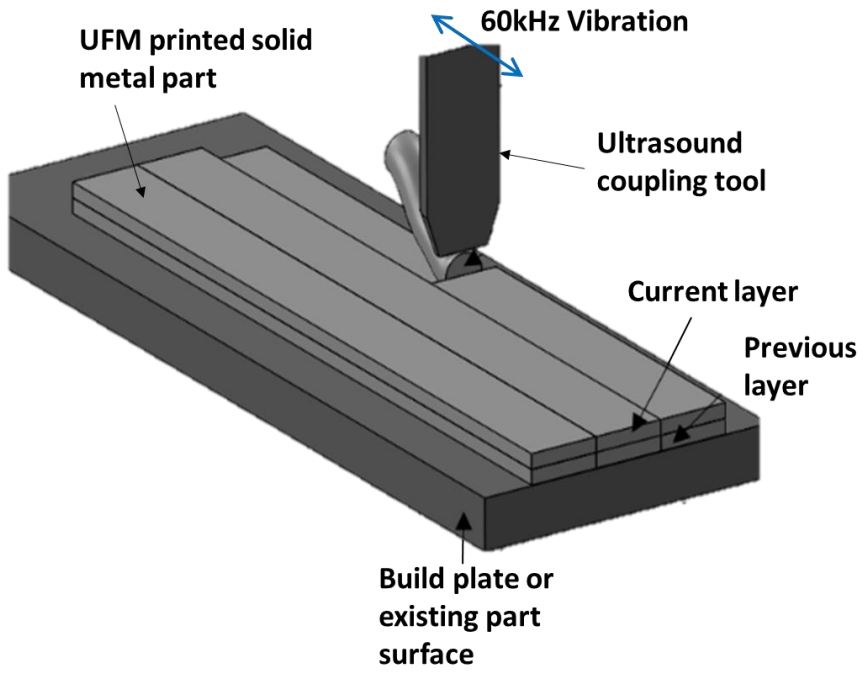

Figure 4: Schematic Diagram of the Process when the 2nd Layer is Being Built

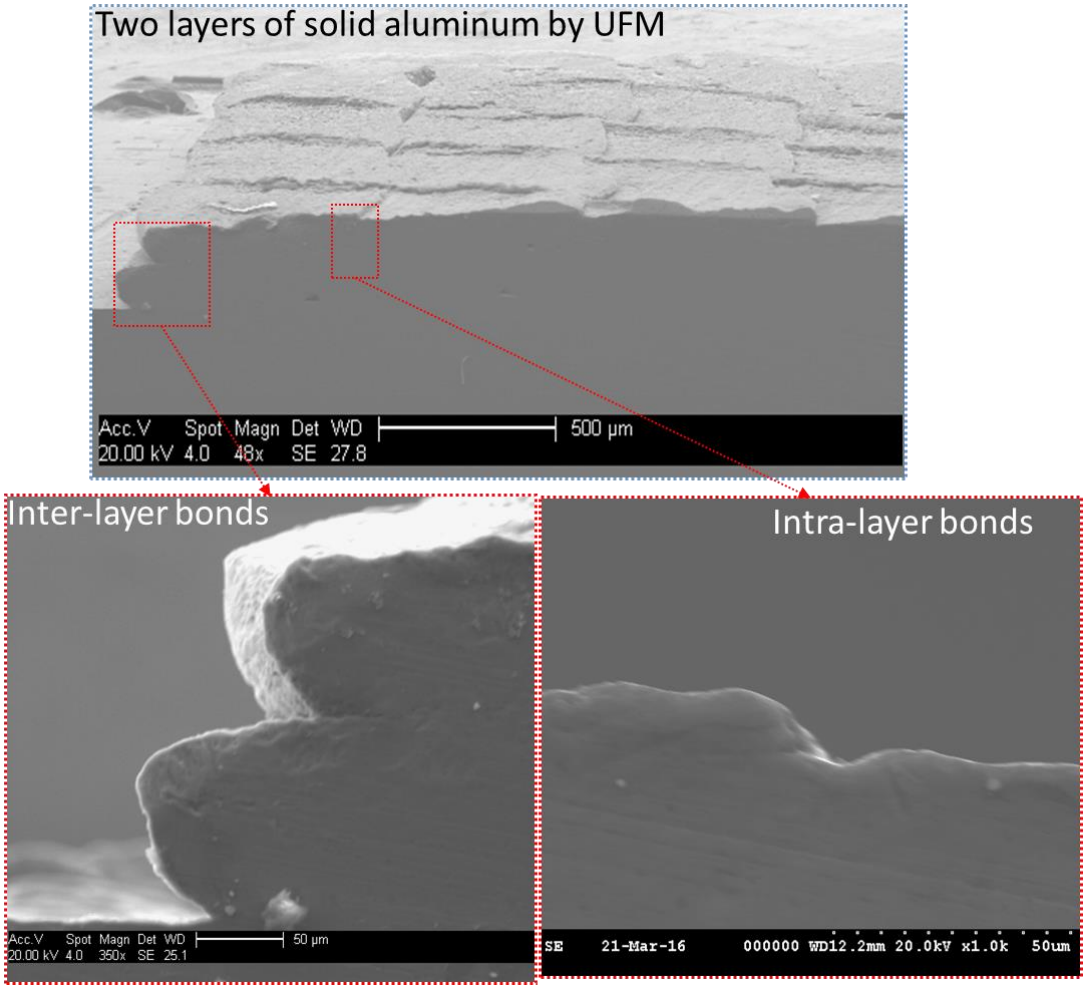

Figure 5: SEM Images of the Cross Section After Two Layers Have Been Built

Temperature measurement during the process

A FLIR A6751 camera was used for IR imaging of the process. The imaging frequency was 125.6 Hz. Black polymeric film was used on part of the tungsten-carbide tool to reduce the reflectivity of the surface. Figure 6 shows the schematic of the IR camera setup during the temperature measurement experiments. To confirm the IR imaging results, thermocouples were used to measure the temperature at 0.6mm and 4mm away from the bonding interface.

The temperature rise in the UFM process can be attributed to three heat sources: (1) the volumetric heat generation from large amounts of plastic deformation associated with the height change in the filament during voxel formation, (2) the frictional heat generated due to the cyclic

relative motion between the filament and the substrate (or an existing filament surface), and (3) the cyclic shear deformation of voxel in the filament axial direction. These sources of heat generation were used as inputs in a Finite Element Model to investigate the transient thermal and heat transfer behavior of the tool-voxel-substrate assembly. The results from the IR camera measurements and the Comsol model have been compared in the Results and Discussion of the thesis report.

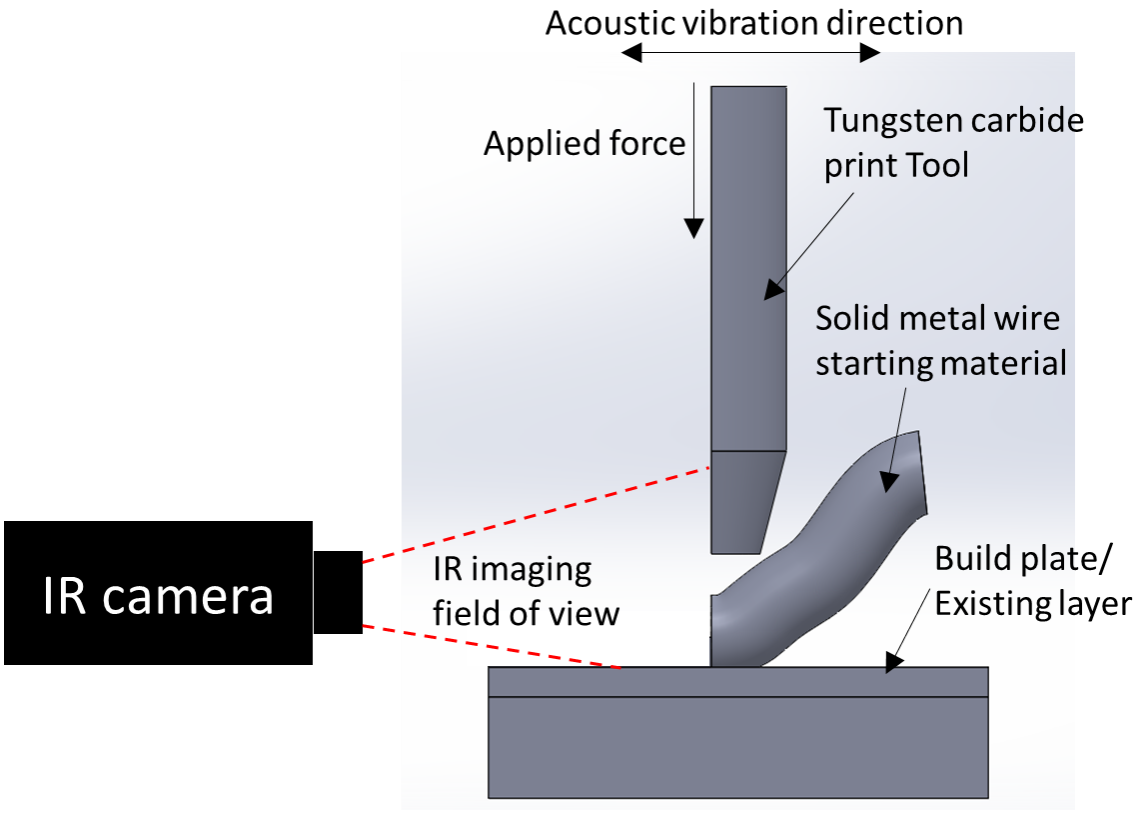

Figure 6: Schematic Diagram of the IR Camera Setup During the Temperature Measurement Experiments

Calculation for the Volumetric Heat Generated During Plastic Deformation

Yield stress of the material, $\sigma_y = \xi K \varepsilon_p^n$ [15]

ξ is the softening factor due to ultrasonic energy, ε_p is the plastic strain and K and n are the material constants.

Interpolation was used to calculate K and n from the values in [15]. K= 155.65 MPa and n=0.2123.

ξ is assumed to be 1 in this case although the value is definitely less than 1. Since the volumetric generation is only a small fraction of the total amount of the total heat generated, the value of ξ will not affect the overall results of the thermal model.

Work done during plastic deformation, $W_p = \int_{h_0}^{h} area \times \sigma_y \times \delta h$

$$= \int_{h_0}^{h} h_o area \times \sigma_y \times \frac{\delta h}{h_0}$$

$$= Volume \times \int_{\varepsilon_0}^{\varepsilon} K\varepsilon^n \times d\varepsilon$$

$$= Volume \times \frac{K(\varepsilon^{n+1} - \varepsilon_0^{n+1})}{n+1}$$

$$Volume = \pi d^2 \times \frac{l}{4}$$

$$=7.07 \times 10^{-11}$$

$$\varepsilon = \ln(\frac{h_0}{h}) = 1.1$$

So, $W_p = 0.01J$

This heat is generated over the 0.3 second time of the process.

Calculation of Frictional Heat Generation

The second source of heat generation is the frictional heating from the relative movements between the voxel and the substrate or the voxel and the tool. If the assumption is made that there is no slip between the tool and the voxel, this can be modeled as $Q_f = \mu FU$ where μ is the coefficient of friction on the voxel-substrate contact, and U is the speed of their relative movements, which is approximated as $U = 4Af$ where A is the amplitude of vibration, f is the

frequency of vibration, and *F* is the contact force [20]. For UFM, a metallurgical bond starts to form at 30 milliseconds into voxel formation after which the relative movement between the filament and the substrate stops. The contact force is 10N, the vibrational amplitude is 0.98 microns, and the frequency is 60 kHz. For the aluminum filament-aluminum substrate interface under irradiation of ultrasound vibration, a friction coefficient of 0.3 is assumed during voxel formation [20]. Based on these values, the total frictional heat generation on the filament-substrate contact is calculated to be 0.7W.

Calculation for the Heat Generated Due to the Cyclic Shear Deformation of Voxel in the Filament Axial Direction

The total shear strain on the voxel is given by the equation, $\varepsilon_s=A/h$, where A is the vibration amplitude and h is the instantaneous height of the voxel. As the filament deforms to form the voxel, the total shear strain changes continuously over the 300 milliseconds time of the process. The deformation of the filament from 300 microns to 100 microns has been divided into short intervals of 10 microns over which the shear strain rate is assumed to remain constant.

For example, for the first interval in which the filament deforms from 300 micron to 290 micron, the total shear strain in the filament is $\varepsilon_s= 1/300=0.03$.

Elastic strain is given by, $\varepsilon_e=\sigma_y/E$, where σ_y is the yield strength of the material and E is the Young's modulus. For aluminium, σ_y = 35MPa and E = 26GPa. Hence, $\varepsilon_e=0.01$

Plastic shear strain is given by $\varepsilon_p=\varepsilon_s- \varepsilon_e=0.002$.

Total strain energy per cycle = $4 \times \varepsilon_p \times \sigma \times$ volume = 1.967×10^{-5} J

Total strain energy per second = Total strain energy x f = 1.18 W, where f is the frequency of vibration.

Assuming 30% of the strain energy is converted to heat, the amount of strain heat generated over a time interval of 0.0143 seconds during which the filament deforms from 300 microns to 290 microns is 0.005 J [21]. Similarly, heat generated over all the intervals is added to calculate the

total heat generation due to cyclic shear deformation of the voxel, which amounts to 0.225 J. Therefore, since 0.225 J of heat is generated over 300 milliseconds, heat generated per second is equal to 0.75 W.

The values of the volumetric heat generation during plastic deformation, heat generated due to the cyclic shear deformation of voxel in the filament axial direction and frictional heat generation were input in the transient model. The results have been discussed in the Results section of the thesis report.

Micro Computed Tomography (Micro-CT) of the UFM Samples

Micro-CT is a high resolution method to observe the internal defect structure of an object non-destructively. A rotating X-ray source illuminates an object with X-rays. An X-ray detector collects magnified projection images of the object taken from several different viewing angles. A computer generates a 3D image from several such 2D images taken from different viewing angles which reveals the internal structure of the sample without destroying the sample.

Micro-CT images of an object made using the UFM process were taken to reveal the defect structure of the sample.

Microstructure Evolution in UFM

To examine the microstructures of aluminum formed by the UFM process, metallography sample preparation and Atomic Force Microscopy were used to characterize the cross-section (normal to the filament axis) of a voxel at three states: un-processed virgin aluminum filament, aluminum voxels formed with two different levels of ultrasonic energy inputs that correspond to a 0.96 and 0.98 micron vibrational amplitudes.

Atomic Force Microscopy (AFM) is a high-resolution surface imaging technique. Figure 7 shows the schematic diagram of AFM. A sharp tip scans the surface of the sample. A laser is incident on the back of the cantilever that carries the tip. As the cantilever deflects due to the undulations on the sample, the changes in the position of the reflected laser are detected by the position

sensitive detector. These deflections of the cantilever are converted to 2D images using computer software.

Aluminum voxels were formed using two different ultrasonic powers (corresponding to amplitudes of 0.96 microns and 0.98 microns respectively) on aluminum 1100 substrates and the microstructures of the formed voxel was examined. After the voxels formed on the substrate, their cross-sections were prepared following standard metallography procedures. The samples were polished with 320 grit silicon carbide abrasive disc followed by 600 grit silicon carbide abrasive disc. Further polishing was performed using 6 µm polycrystalline diamond particles followed by 0.05 µm alumina slurry. Between each polishing step, sample were cleaned in an ultrasonic DI water bath. After the polishing process, the samples were etched in an etchant containing 25ml methanol, 25ml HCl, 25 ml nitric acid and 1 drop HF. The etched samples were examined on a Bruker Multimode Atomic Force Microscope to reveal the microstructure of the aluminum voxels under different ultrasonic power inputs. Same procedure was also used to prepare the raw aluminum filament as a control sample. ImageJ software was used to measure the grain size of the sub-grains in the obtained images.

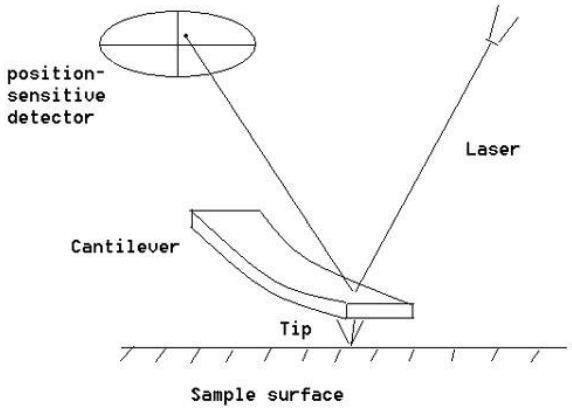

Figure 7: Schematic Diagram for AFM

Enhanced Mass Transport Analysis

To analyze the large amount of mass transport across the filament-filament or filament-substrate interface during the UFM process, two pure aluminium voxels were bonded to a pure copper substrate. Different ultrasonic power amplitudes of 0.96 micron and 0.98 micron were used to bond the two voxels. A cross-section of each of the samples was cut to expose the aluminium-copper interface. The samples were polished using the same polishing procedure used for the microstructure analysis. After polishing, an Energy Dispersive Spectroscopy (EDS) line scan was performed at the interface. For the scans on both the samples, same accelerating voltage and the magnification was used. ZAF correction was used to account for atomic number (Z), absorption (A) and fluorescence (F) effects.

In EDS, a high energy electron beam is accelerated on the sample. The incident beam interacts with the electrons in the sample and excites them which ejects them from their inner shell creating an electron hole. An electron from an outer shell can which has higher energy state fills the hole in the shell which has lower energy state. In the process, the energy difference in the two electron shells is emitted in the form of X-rays. These X-rays are characteristic to the two electron shells and to the atoms. These X-rays are detected by an energy-dispersive spectrometer to determine the elemental composition of the sample. Figure 8 shows the schematic diagram of an EDS system in an SEM.

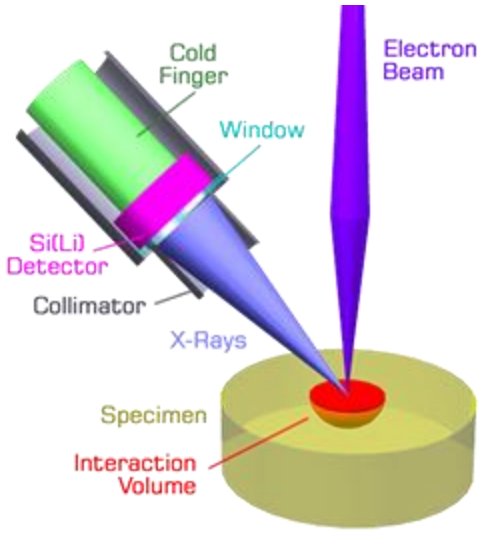

Figure 8: Schematic for the Energy Dispersive Spectroscopy

A EDS line scan divides a line into known number of points and measures the atomic count of elements at each point on the line. To analyze the mass transport across the aluminium-copper interface, an EDS line scan was performed to observe the gradual change in the atomic counts of aluminium and copper along the line. Figure 9 shows the SEM during the EDS line scan.

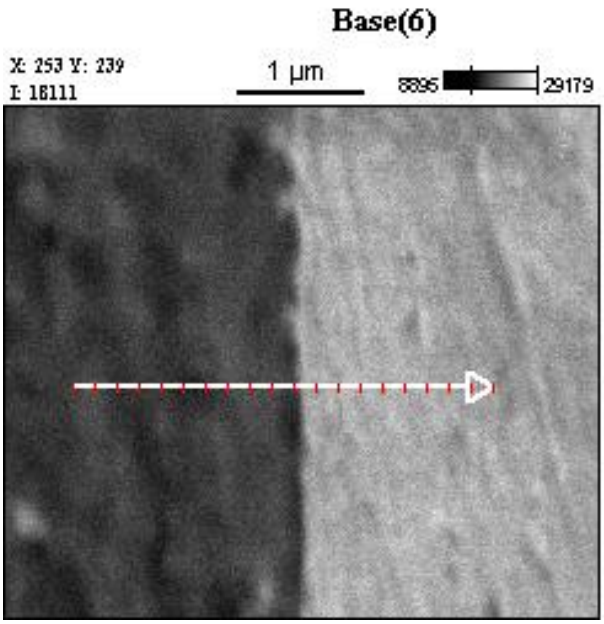

Figure 9: Line Scan Across the Aluminum-Coper Interface

4. RESULTS

Ultrasonic Filament Modeling as a Stand-Alone 3D Printing Process

Using the experimental setup and methodology for UFM explained in the earlier section, millimeter scale components were printed. Figure 10 shows an L-shaped object printed using the UFM process. As shown in the figure, the object is 5mm long, 4mm wide and approximately 1.5 mm tall with a layer height of 125 microns. To further prove the ability of the process in a stand-alone mode, few more millimeter scale objects were printed. One such object has been shown in Figure 11. Surface defects observed on the sample are a courtesy of the current wire locating mechanism. Further engineering development of the experimental setup and process will help in improving the geometrical accuracy of the manufactured components.

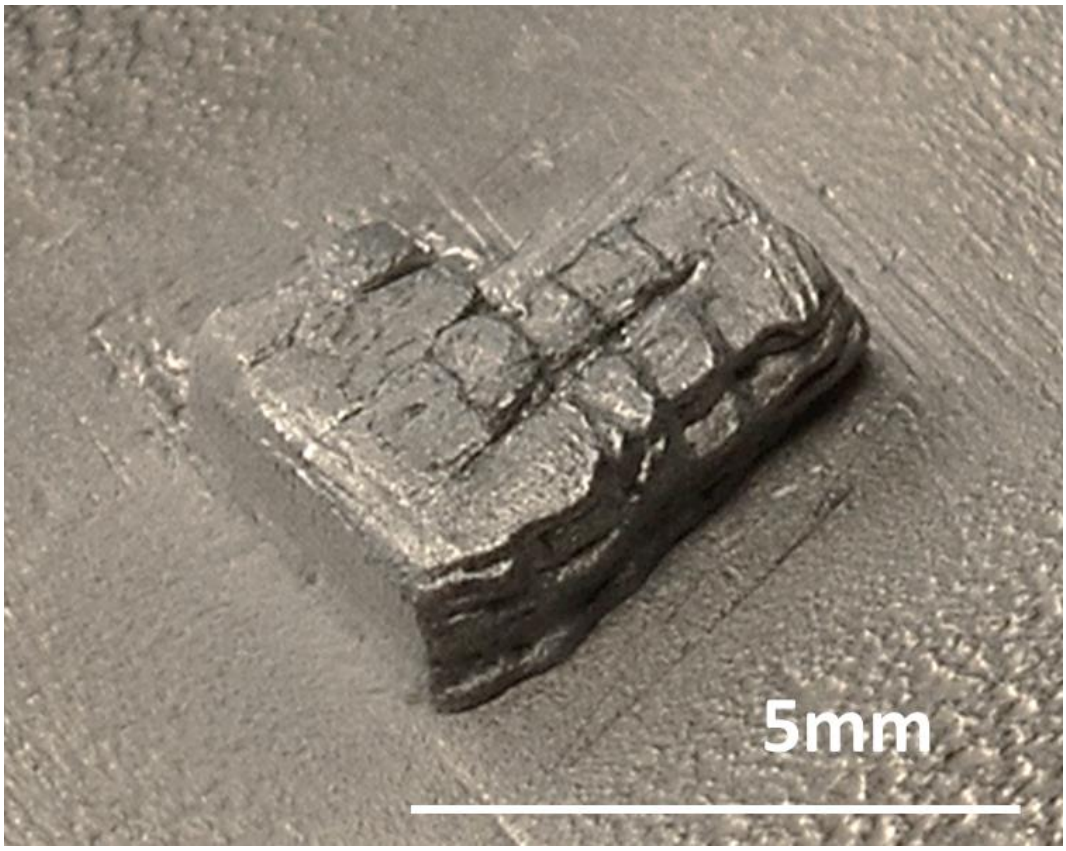

Figure 10: L-Shaped Article Printed with the UFM Process

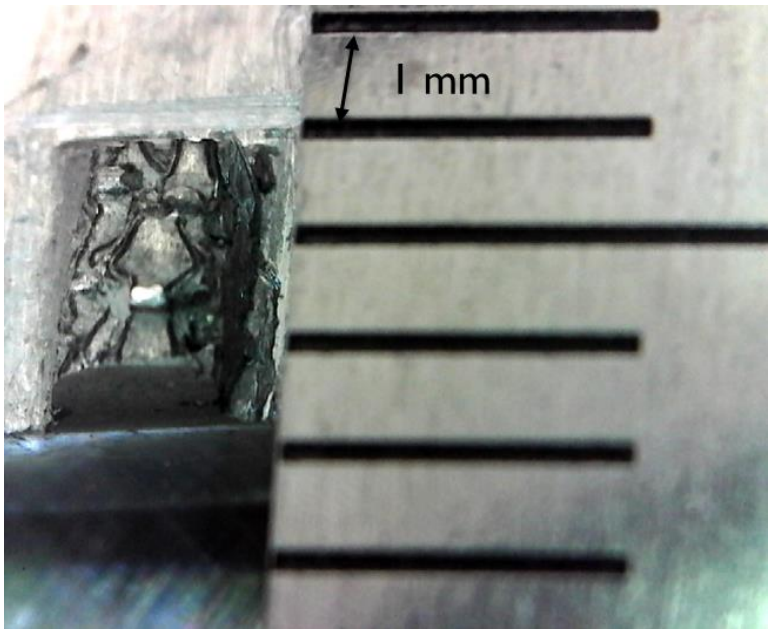

Figure 11: Sample Printed Using UFM Process in Stand-Alone Mode

Ultrasonic Filament Modeling as a Hybrid 3D Printing Process

To demonstrate implementation of UFM as a hybrid additive-subtractive manufacturing process, a 16 layer- aluminum structure was 3D printed and machined down to a tensile bar-shaped object. Figure 12 shows the tensile-bar shaped after the machining operation. Using similar process, a simple cube was manufactured. Figure 13 shows the cube.

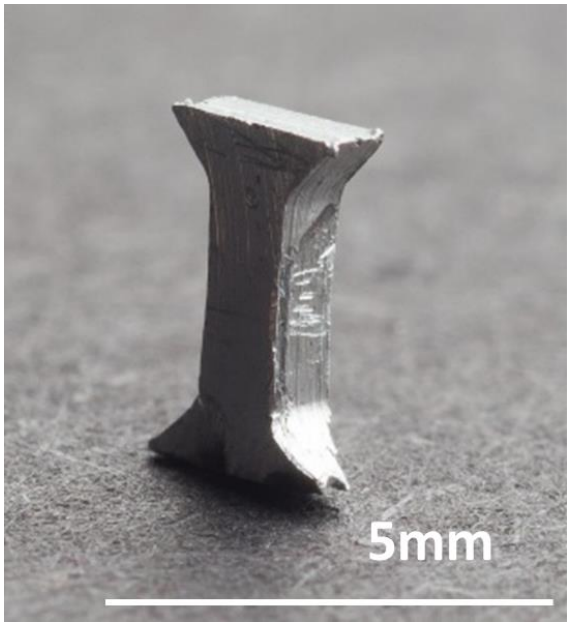

Figure 12: Tensile Bar-Shaped Object Manufactured Using the UFM Process in Hybrid Mode

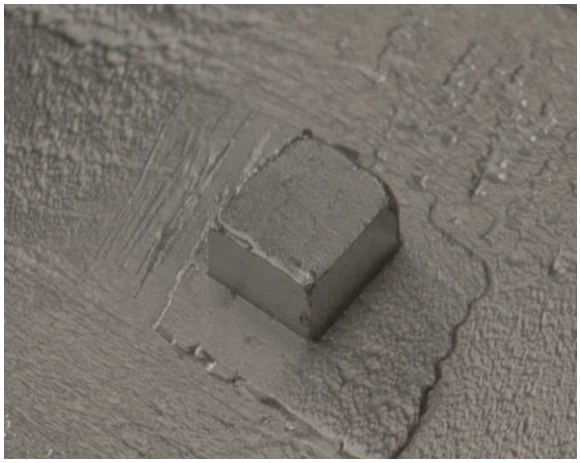

Figure 13: A Simple Cube Manufactured Using UFM in Hybrid Mode

Micro-CT of the UFM Samples

Figure 14 shows the micro-CT results of the dog-bone shaped sample printed using UFM in hybrid mode. Image on the right shows a slice of the of cross-section of the sample. The resolution of the micro-CT scan is 1 micron.

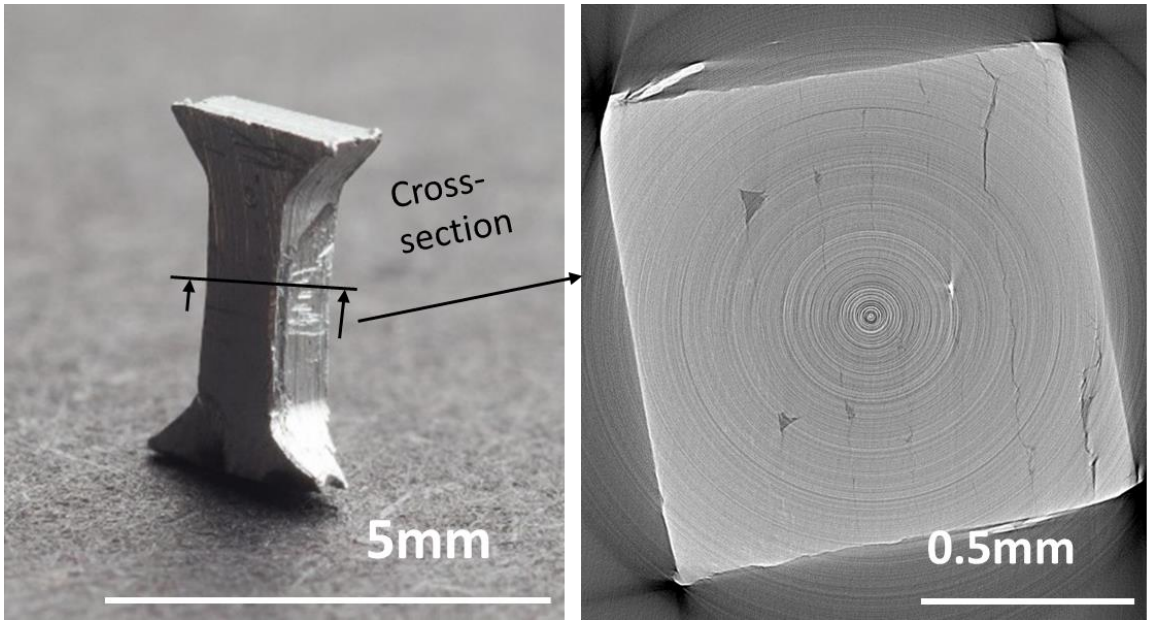

Figure 14: Micro-CT Results of the Dog-Bone Shaped Sample Printed Using UFM in Hybrid Mode

Temperature Evolution During UFM Process

In Figure 15 one frame of thermal video captured during voxel formation shows the spatial temperature distribution in the vicinity of the voxel at the time the maximum temperature is reached. a plot of maximum temperature in during the process versus time. Maximum temperature rise of about 5.2°C was seen. In the temporal plot, the ultrasonic irradiation starts at 50 milliseconds. The temporal plot indicates that the maximum temperature is reached within the first 25-30 milliseconds after the ultrasonic irradiation starts and the temperature gradually decreases after that. Another feature in the temporal temperature profile is the sharp reduction at 350 microseconds where the ultrasonic vibration stops. This indicates the removal of the second heat source in the process: cyclic plastic strain heating due to the high-frequency cyclic shear deformation in the voxel as it forms. These results have been further discussed in the next section.

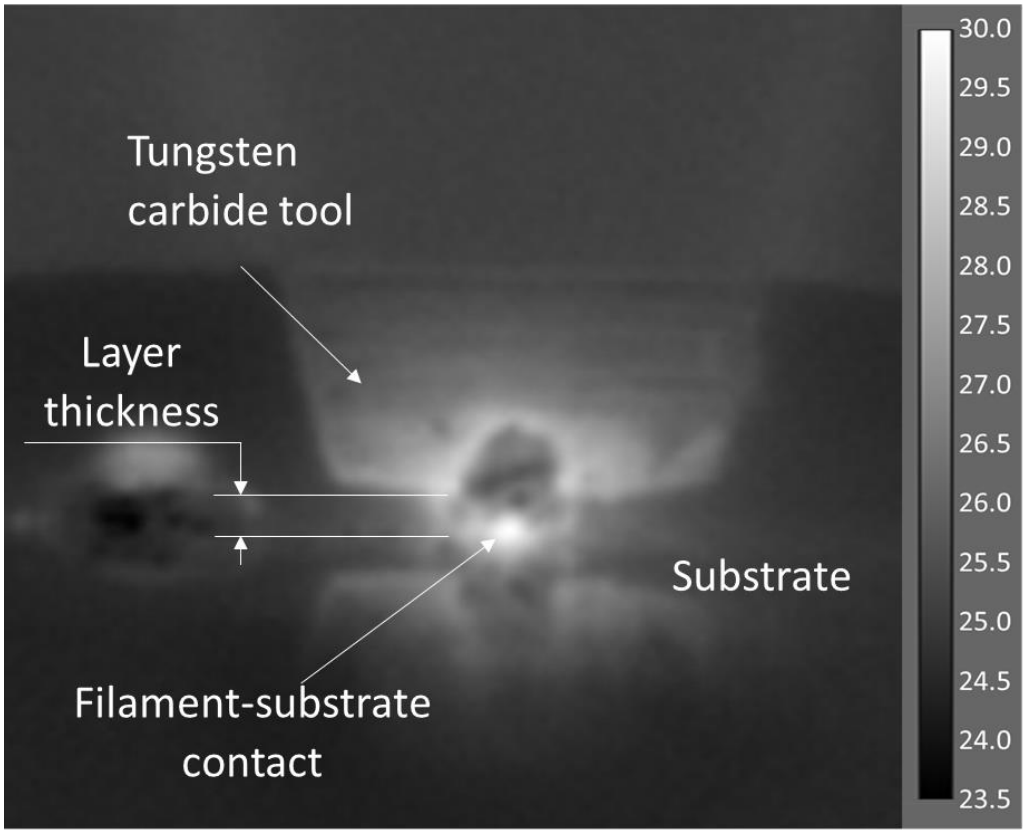

Figure 15: IR Image at the Instant when Maximum Temperature is Recorded During the UFM Process

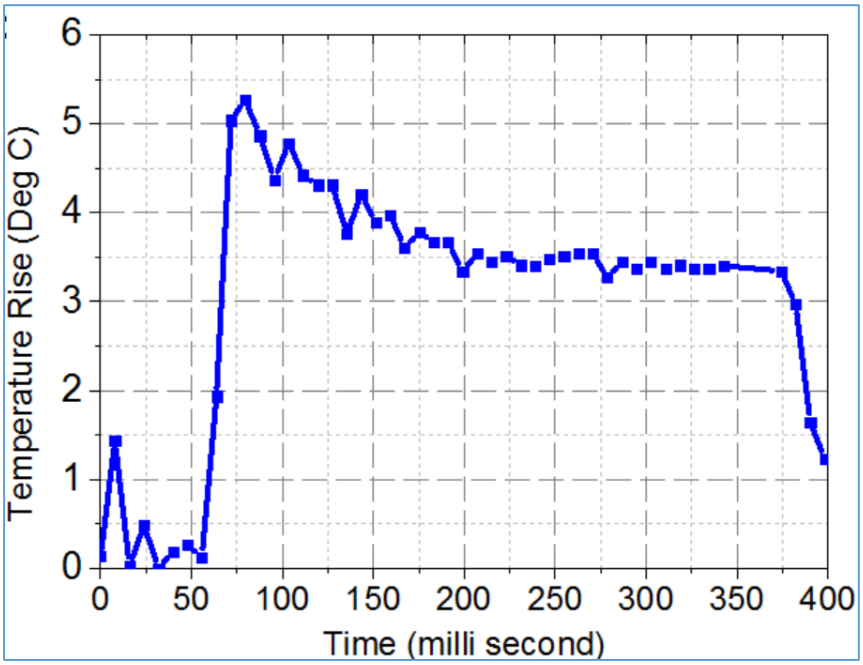

Figure 16: Plot Showing the Evolution of Temperature Versus Time Recorded Using IR Imaging

The values of all three types of heat generation during the voxel forming and bonding process were input in the Finite Element Analysis (FEA) model to analyze the temperature at the interface during voxel formation and bonding. Figure 17 shows the plot of evolution of temperature versus time obtained from the FEA model and Figure 18 shows the graphical image of the instant when the maximum temperature is seen during the process. The plot shows a temperature rise of 5^0 C and the sudden drop in temperature after 0.3 seconds when the ultrasonic irradiation stops.

Thermocouple measurements at a distance of 0.9 mm and 4.3 mm away from the center of the voxel show a temperature rise of 1.9^0 C and 0.33^0 C respectively. These values of temperature corroborate the IR imaging and the thermal model results.

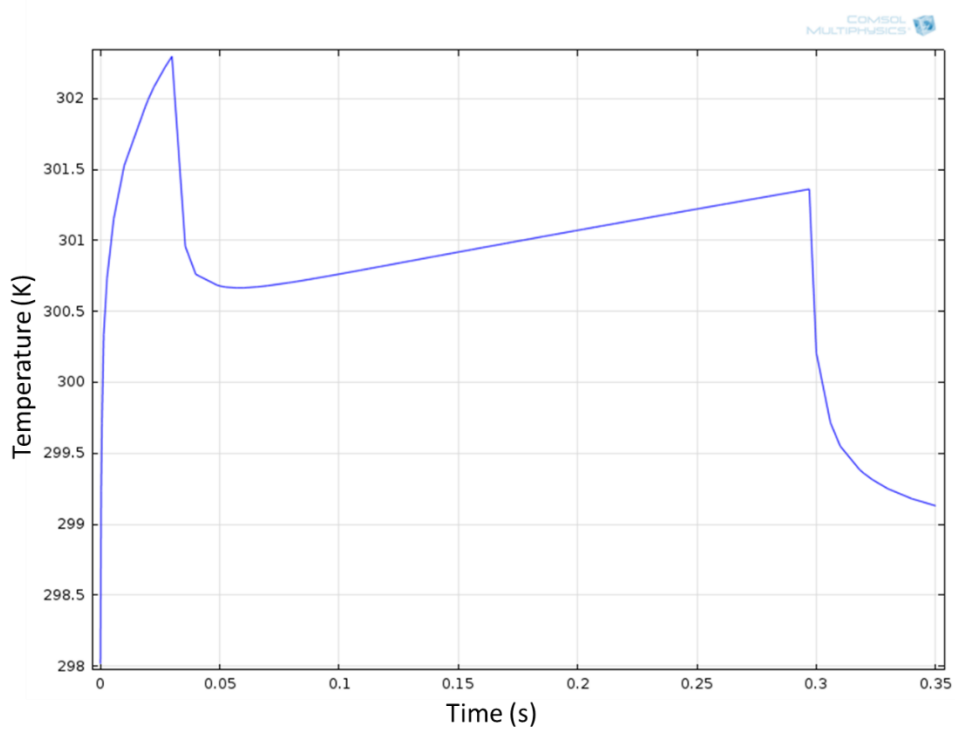

Figure 17: Plot Showing the Evolution of Temperature Versus Time Recorded Using FEA Model

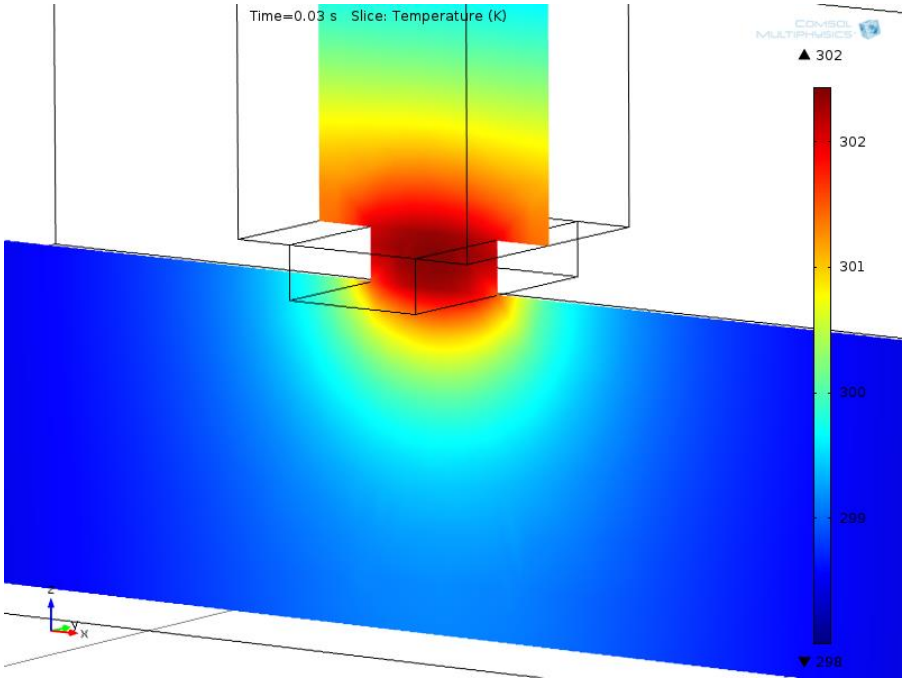

Figure 18: Graphical Image from the FEA Model at the Instant When Maximum Temperature is Seen in the UFM Process

Microstructure Evolution in UFM

Figure 17 shows the AFM image of the micro-structure of an un-processed virgin aluminum filament, aluminum voxels formed with ultrasonic energy input corresponding to 0.96 micron vibration amplitude, interface region of the aluminium voxels formed with ultrasonic energy input corresponding to 0.96 micron vibration amplitude and aluminum voxels formed with ultrasonic energy input corresponding to 0.98 micron vibrational amplitudes. The virgin filament, in Figure 17a, shows an average grain size of approximately 10 microns, whereas both of the formed voxels show formation of sub-grains within the primary grains. Grain size analysis performed in ImageJ shown in Figure 18 shows that the primary grains remain approximately the same size, they are deformed as a result of the plastic strain in the voxels. Further, at the lower ultrasound energy input, the sub-grains have an average size of 1.4 microns while the average sub-grain size at increased ultrasound input reduces to 0.9 microns. In Figure 17c, the microstructure of a voxel in the interface region is shown. There are no discernable differences in morphology compared with morphology observed within the voxel in that the microstructures in different regions are characterized by large (~10 microns) deformed primary grains within which the formation of sub-grains of roughly 0.9 micron in size are observed. This indicates that once a voxel is formed the morphology across the interfaces and within voxels remains uniform.

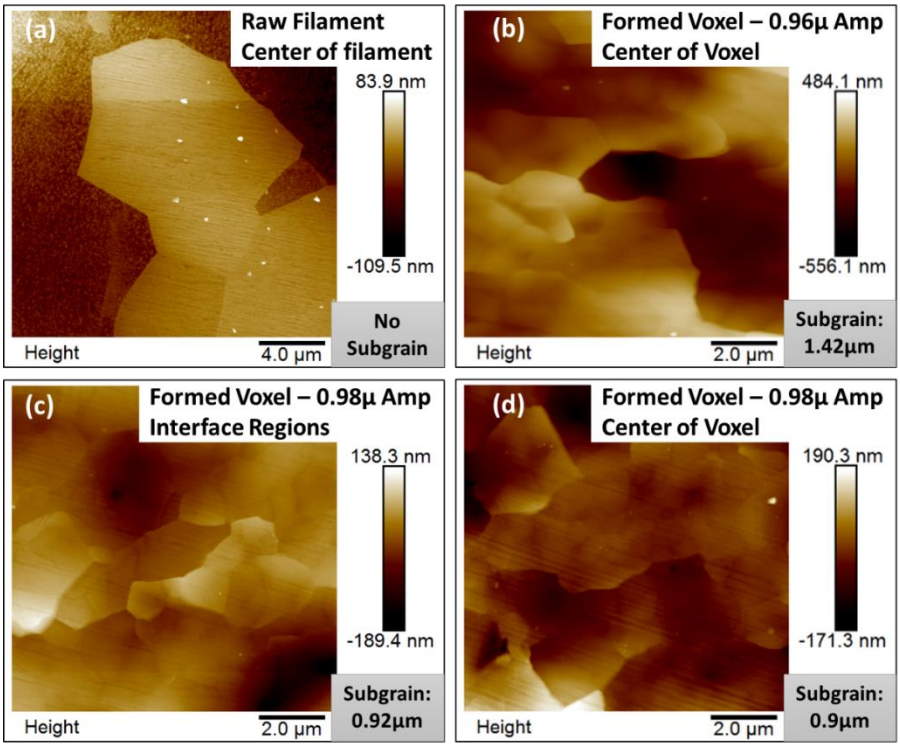

Figure 19: AFM Images Showing Evolution of Microstructure as the UFM Process Occurs

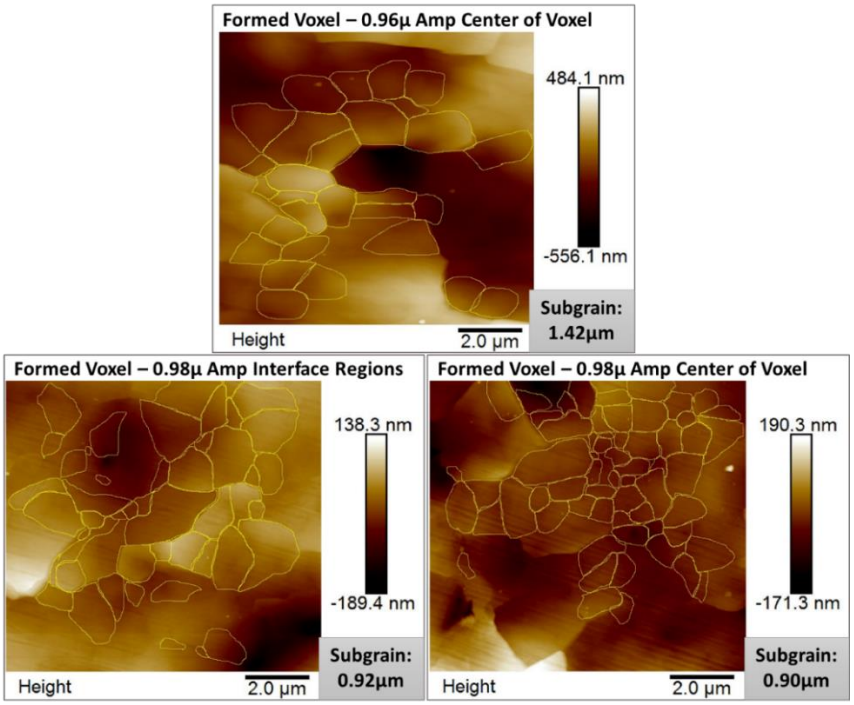

Figure 20: Microstructure of the UFM Samples After Grain Size Analysis Performed in Imagej Software

Enhanced Mass Transport Analysis

Figure 19 and Figure 20 show the results of the EDS line scan at the interface of the voxel-substrate interface formed using ultrasonic energy density corresponding to the vibration amplitude of 0.96 micron and 0.98 micron respectively. The interface is the region with a mixture of aluminium and copper atoms caused by the mass transport of atoms from one region into other. Hence, when moving towards the interface from the aluminium region, a gradual decrease in the percentage aluminium count can be seen until it becomes zero in the copper region. A similar trend is seen in the percentage copper count when moving towards the interface from the copper region. For the sample with ultrasonic energy density corresponding to the vibration amplitude of 0.96 micron, the interface thickness was measured to be 1188.4 nanometers and for the sample with ultrasonic energy density corresponding to the vibration amplitude of 0.98 micron, the interface thickness was measured to be 1365 nanometers.

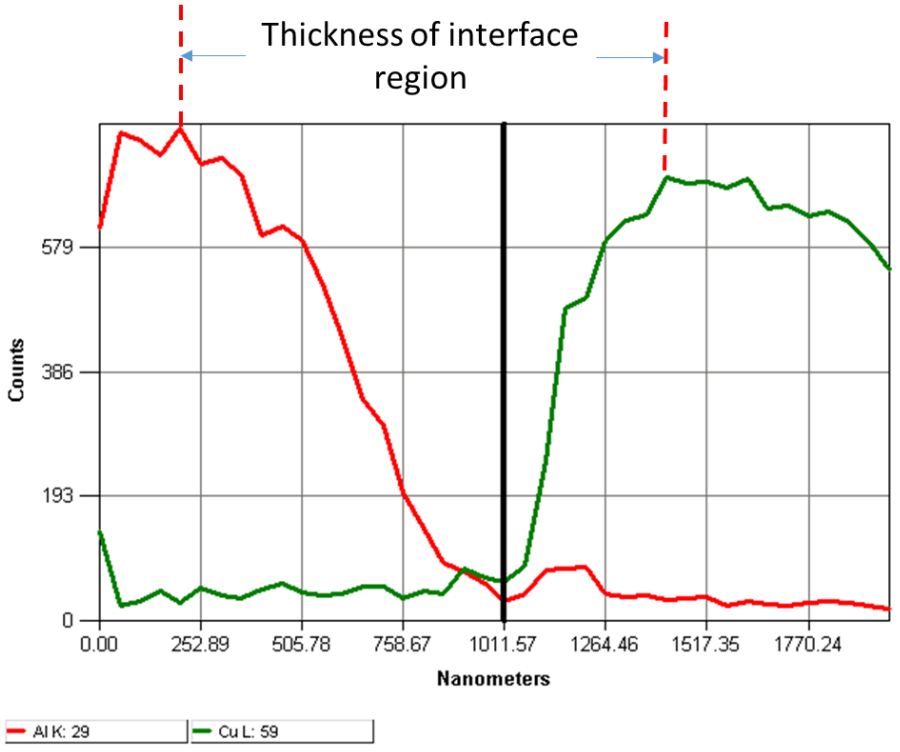

Figure 21: EDS Line Scan Results for the Interface of the Sample Formed Using Ultrasonic Energy Density Corresponding to Vibration Amplitude of 0.96 Micron

It can be seen that for higher ultrasonic energy densities, the interface thickness is greater indicating greater amount of mass transport. These results provide a qualitative analysis of the interface region which indicates that mass transport increases with increase in ultrasonic energy density.

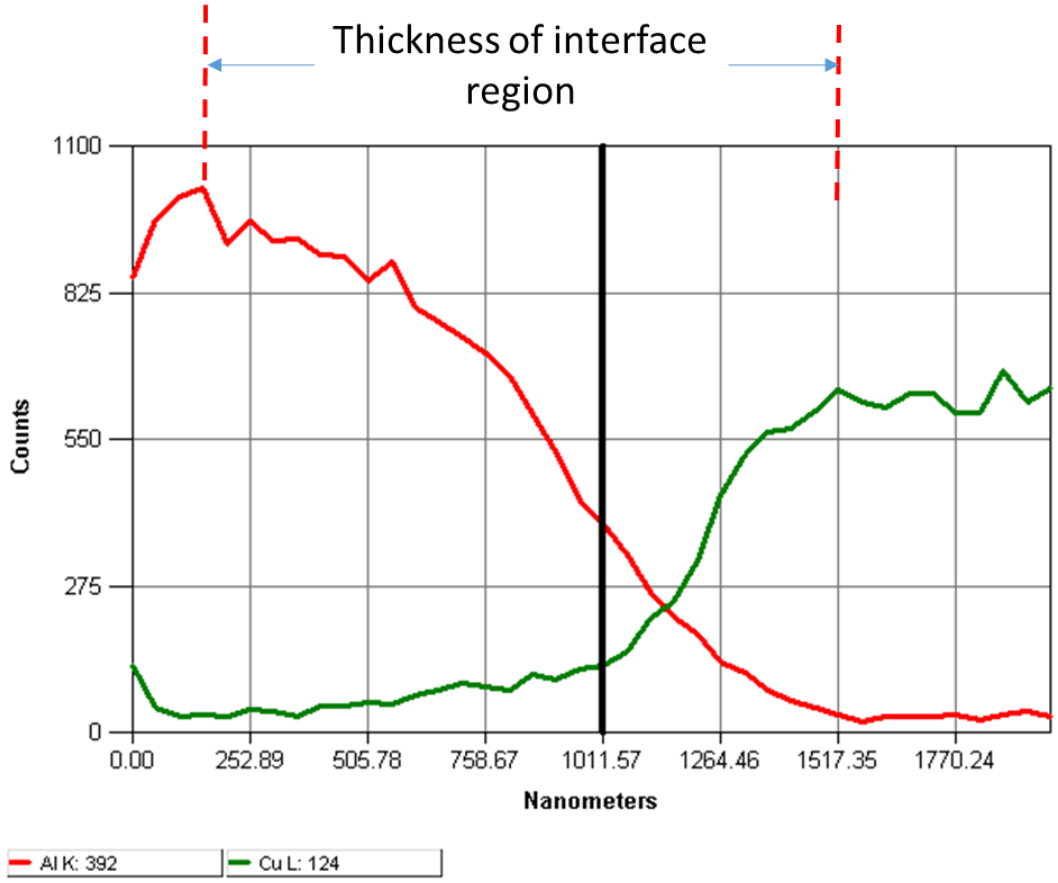

Figure 22: EDS Line Scan Results for the Interface of the Sample Formed Using Ultrasonic Energy Density Corresponding to Vibration Amplitude of 0.98 Micron

5. DISCUSSION

Ultrasonic Filament Modeling as a 3D Printing Process

The millimeter scale objects printed provide a proof of concept for the UFM process as a feasible ambient condition and room temperature metal additive manufacturing process. It can be stand-alone metal additive manufacturing process which does not require post processing operation to print fully dense (>95%) metal components and it can also work in hybrid mode to manufacture precise components. Since it uses filament as starting material, it can eliminate the process hazards associated with the using powders as starting material. Due to its distinct advantages, it can be implemented in a desktop 3D printer environment. Being a room temperature process, it can make manufacturing of polymer-metal composites possible. It has the potential to make metal additive manufacturing affordable and accessible by reducing the initial setup and equipment costs.

Micro-CT of the UFM Samples

SEM images in Figure 5 show that there is no discernible inter-filament or inter layer interface. In the micro-CT images in Figure 14 of the UFM samples, inter-layer interfaces are somewhat discernible but the inter-filament interfaces are not and over 95% density is observed indicating that UFM does not require any post processing operation to manufacture fully dense metal components. The circular pattern on the micro-CT images are an artifact of the micro-CT imaging technique. Both these sets of images indicate that there is inter-filament lateral mass transport and inter-layer build-direction mass transport also. This enables to reduce the anisotropy in the components manufactured using UFM.

Temperature Evolution During the UFM Process

As shown in Figure 16, the voxel formation process starts at 50^{th} millisecond with the beginning of irradiation of ultrasound. During the initial 30 milliseconds of the voxel forming process, the relative movements between the two surfaces provide frictional heating that results in the sharp temperature rise. After about 30 milliseconds, the metallurgical bond starts to form and the relative movements between the filament and substrate stops. This removes the frictional heat

source and allows the interface temperature to drop. A maximum temperature rise of 5 degrees is observed. After about 300 milliseconds after the beginning of ultrasound irradiation, the ultrasound irradiation stops. This stops the heat generation due to cyclic plastic deformation caused by the ultrasonic vibrations. Hence, a 2nd sharp drop in the interface temperature can be seen.

The average total heat generation due to cyclic plastic deformation during voxel formation is 0.75W, that due to frictional heat generation on the filament-substrate contact is 0.7W and the volumetric heat generated due to plastic deformation associated with the height change in the filament during voxel formation is 0.01 W. The total amount of heat generated during the voxel formation and bonding process is about 1.46 W. The heat generation due to cyclic plastic deformation during voxel formation accounts for 51.36% of the total heat generated, frictional heat generated accounts for 47.9% of total heat generated and volumetric heat generated due to plastic deformation associated with the height change in the filament during voxel formation accounts for only 0.68% of the total heat generated.

Microstructure Evolution During the UFM Process

The microstructure of a formed aluminum voxel via UFM shows a microstructure similar to what is commonly observed in dynamic recovery of aluminum. Dynamic recovery can take place in hot working conditions ($T > 50\% T_m$), in strains of less than $\varepsilon = 40$. This behavior is typically seen in materials with high stacking fault such as aluminum and titanium [22] [18] [19]. One distinct characteristics is the formation of subgrains within primary grains as a result of formation of small angle grain boundaries as dislocations accumulate within primary grains. In UFM similar microstructural evolution is observed. However, the UFM process takes place at room temperature ($T < 5\% T_m$), and the amount of strain experienced in the voxels is approximately $\varepsilon = 1$. In addition, it is observed that the extent to which this microstructural evolution process takes place increases as the ultrasonic energy input into the voxel increases. Although these observations suggest that the driving mechanism behind the microstructural evolution observed in UFM differs from those in dynamic recovery, the trend illustrating microstructural dependence on

ultrasonic energy input is similar to that in dynamic recovery whereas the working temperature increases, a decrease in subgrain size is observed [22]. We propose that from an energetics' perspective, this trend suggests that the irradiation of ultrasonic energy allows the material lattice to reach a higher energy state where the dynamic recovery due to dislocation hopping and merging can occur readily as if the temperature of the materials is raised.

In the context of UFM as a metal 3D printing process, this dependence of material microstructure on process input means the mechanical properties of 3D printed parts can be controlled and tuned in real-time during the building process by understanding and controlling the process physics.

Enhanced Mass Transport Analysis

The results shown in the last section show that there is an increase in the size of the interface indicating an increased mass transport across the interface with an increase in ultrasonic power used during the voxel formation and bonding process.

The characteristics X-rays used by EDS to measure the atomic percentage are derived from a volume of the sample as shown in Figure 21. This interaction volume will cause the results of interface mass transport to be skewed and will show an exaggerated size of the interface. Hence, these EDS results are not sufficient to model and fully understand the process physics behind enhanced mass transport. However, the interaction volume depends on the accelerating voltage in keV, critical excitation energy in keV and mean specimen density in g/cc. By keeping all these parameters constant while analyzing all the samples, the size of the interaction volume was kept constant. This has enabled to get a relative measure of the increase in the interface thickness with an increase in ultrasonic power.

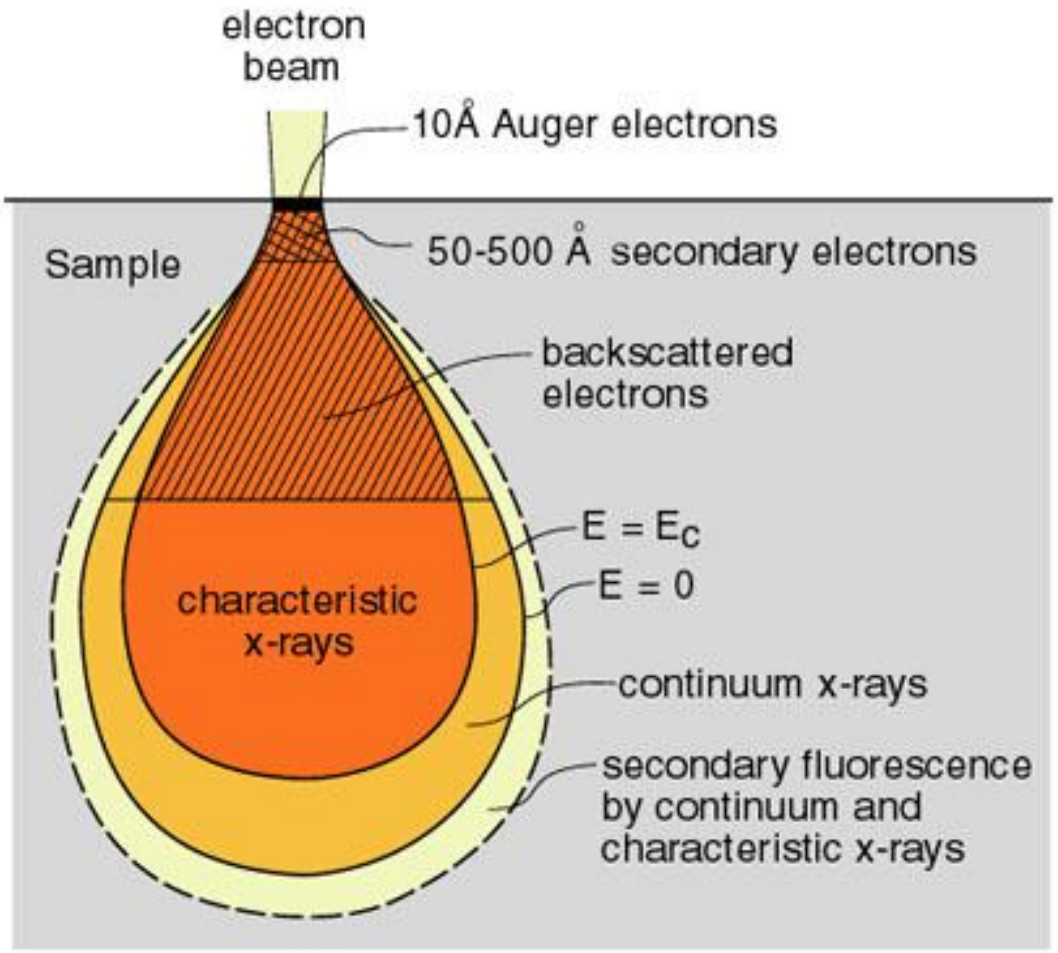

Figure 23: Schematic Illustration of Interaction Volumes for Various Electron-Specimen Interactions

6. FUTURE WORK

1. In this research work, process feasibility of UFM as a 3D printing process has been demonstrated by printing millimeter scale articles. The articles have surface defects caused by the imprecise experimental setup. Improvements to the overall experimental setup will help in improving the part quality and surface finish.
2. The research work presents a preliminary analysis of the evolution of micro-structure during the process. A more detailed analysis using Electron Backscatter Diffraction Method (EBSD) will provide the complete understanding of the microstructure evolution during the process.
3. Although a significant amount of research has gone into studying the ultrasonic softening of metals, studying the process in the context of UFM is essential to achieve accurate and desirable amount of voxel deformation.
4. The process physics behind mass transport occurring during the voxel formation and bonding has not been fully understood. It needs to be studied using methods like TEM which will eliminate the issues with interaction volume.
5. Several other materials like titanium that are difficult to work with using the current additive manufacturing processes need to be tried to expand the process scope.

7. SUMMARY

The research work provides proof of concept for the Ultrasonic Filament Modeling process which can additively manufacture fully dense metal components at room temperature and ambient conditions using ultrasonic energy. The research work demonstrates the experimental setup and methodology of the UFM process.

The temperature evolution during the process has also been studied in this work. The maximum temperature rise during the process measured using IR imaging was found to be 5^0 C. Temperature evolution can be attributed to three heat sources during the process- (1) the volumetric heat generation from large amounts of plastic deformation associated with the height change in the filament during voxel formation, (2) the frictional heat generated due to the cyclic relative motion between the filament and the substrate (or an existing filament surface), and (3) the cyclic shear deformation of voxel in the filament axial direction. A FEA model was prepared to validate the results of IR imaging. Thermocouple measurements of temperature done at 2 different locations on the substrate corroborate the results of IR imaging and FEA model.

Two parallel phenomenon of ultrasonic softening and enhanced mass transport enable the voxel forming and shaping during the process. To understand the ultrasonic softening phenomenon, the microstructure evolution during the process has been studied. The characteristics of the microstructure were found to be similar to that during the hot deformation of aluminium with the formation of sub-grains.

EDS analysis of the aluminium-copper interface were done to understand the process physics of enhanced mass transport. An increase in the interface thickness was seen with an increase in ultrasonic power used during voxel formation and bonding indicating to an increase in the mass transport, but quantitative analysis of the results could not be done due to the interaction volume associated with the EDS results.

REFERENCES

[1] D. L. Bourell, M. C. Leu and D. W. Rosen, "Roadmap for Additive Manufacturing Identifying the Future of Freeform Processing," in *International Solid Freeform Fabrication Symposium*, Austin, Texas, 2009.

[2] S. Mellor, L. Hao and D. Zhang, "Additive manufacturing: A framework for implementation," *Internation Journal of Production Economics,* pp. 194-201, 2014.

[3] N. Guo and M. C. Leu, "Additive Manufacturing: technology, applications and research needs," *Front. Mech. Eng,* vol. 8, no. 3, pp. 215-243, 2013.

[4] I. Campbell, D. Bourell and I. Gibson, "Additive manufacturing: rapid prototyping comes of age," *Rapid Prototyping Journal,* vol. 18, no. 4, pp. 255-258, 2012.

[5] D. D. Gu, W. Meiners, K. Wissenbach and R. Poprawe, "Laser additive manufacturing of metallic components: materials, processes and mechanisms," *Internation Materials Reviews,* vol. 57, no. 3, pp. 133-164, 2012.

[6] U. Geibler, M. Schneider-Ramelow, K.-D. Lang and H. Reichl, "Investigation of microstructural processes during ultrasonic wedge/wedge bonding of AlSi1 wires," *Journal of Electronic Materials,* vol. 35, no. 1, 2006.

[7] B. Langenecker, "Effects of Ultrasound on Deformation Characteristics," *IEEE Transasction of sonics and ultrasonics,* Vols. SU-13, no. 1, March 1966.

[8] A. Rusinko, "Analytical description of ultrasonic hardening and softening," *Ultrasonics,* vol. 51, pp. 709-714, 2011.

[9] E. S. Amir Siddiq, "Ultrasonic-assisted manufacturing processes: Variational model," *Ultrasonics,* vol. 52, pp. 521-529, 2012.

[10] G.-Y. K. Z. W. L. F. Q. Z. D. M. Z. C. Zhehe Yao, "Acoustic softening and residual hardening in aluminum: Modeling," *International Journal of Plasticity,* vol. 39, pp. 75-87, 2012.

[11] J. A. George G. Harman, "The Ultrasonic Welding Mechanism as Applied to," *IEEE Transaction on parts,* Vols. PHP-13, no. 1, December 1977.

[12] K. C. Joshi, "The formation of ultrasonic bonds," *Welding Journal,* pp. 840-848, December 1971.

[13] W. F. L. H. J. Z. Junhui Lei, "Theoretical and experimental analyses of," *JOURNAL OF PHYSICS D: APPLIED PHYSICS,* vol. 41, 2008.

[14] M. L. J.-M. K. D.-W. K. C. W. Hongjun Ji, "Nano features of Al/Au ultrasonic bond interface observed by," *Materials Characterization,* vol. 59, pp. 1419-1424, 2008.

[15] S. G. A. J. W. G. J. T. A. B. Gregory S. Kelly, "A model to characterize acoustic softening during ultrasonic consolidation," *Journal of Materials Processing Technology,* vol. 213, pp. 1835-1845, 2013.

[16] E. G. Amir Siddiq, "Thermomechanical analyses of ultrasonic welding process using," *Mechanics of Materials,* vol. 40, pp. 982-1000, 2008.

[17] J. Sietins, J. Gillespie and S. Advani, "Transmission electron microscopy of an ultrasonically consolidated copper-aluminum interface," *Journal of Materials Research,* vol. 29, no. 17, pp. 1970-1977, 2014.

[18] T. Sakai, A. Belyakov, R. Kaibyshev, H. Miura and J. J. Jonas, "Dynamic and post-dynamic recrystallization under hot, cold and severe plastic deformation conditions," *Progress in Material Science,* vol. 60, pp. 130-207, October 2013.

[19] K. W. Siu, A. Ngan and I. P. Jones, "New insight on acoustoplasticity – Ultrasonic irradiation enhances subgrain formation during deformation," *Plasticity,* vol. 27, pp. 788-800, 2011.

[20] J. W. G. J. S. G. A. T. A. B. Steve Koellhoffer, "Role of friction on the thermal development in ultrasonically consolidated aluminum foils and composites," *Journal of Materials Processing Technology,* vol. 211, no. 11, pp. 1864-1877, November 2011.

[21] J. Hodowany, G. Ravichandran, A. J. Rosakis and P. Rosakis, "Partition of plastic work into heat and stored energy in metals," *Experimental Mechanics,* vol. 40, no. 2, pp. 113-123, 2000.

[22] H.J.McQueen, "Elevated temperature deformation at Forming rates of 10^-2 to 10^2 s^-1," *Mettalurgical and material transactions,* vol. 33A, pp. 347-362, February 2002.